A Molecular Basis for the Selectivity of Thiadiazole Urea Inhibitors with Stromelysin-1 and Gelatinase-A from Generalized Born Molecular Dynamics Simulations

Robert C. Rizzo, Samuel Toba,[†] and Irwin D. Kuntz*

Department of Pharmaceutical Chemistry, University of California at San Francisco, San Francisco, California 94143-2240

Matrix metalloproteinases (MMPs) represent a potentially important class of therapeutic targets for the treatment of diseases such as cancer. Selective inhibition of MMPs will be required given the high sequence identity across the family and the discovery that individual MMPs also regulate the natural angiogenesis inhibitor angiostatin. In this study, we have used computational methods to model the selectivity for six thiadiazole urea inhibitors with stromelysin-1 and gelatinase-A, two homologous MMPs that have been implicated in breast cancer. From continuum Generalized Born molecular dynamics (GB-MD) and MM-GBSA analysis, we estimated ligand free energies of binding using 200 snapshots obtained from a short 40 ps simulation of the relevant protein−ligand complex. The MM-GBSA free energies, computed from the continuum GB-MD trajectories, show strong correlation with the experimental affinities ($r^2 = 0.74$); prior studies have employed explicit water MD simulations. Including estimates for changes in solute entropy in the binding calculations slightly diminishes the overall correlation with experiment ($r^2 = 0.71$). Notably, in every case, the simulation results correctly predict that a given ligand will bind selectively to stromelysin-1 over gelatinase-A which is gratifying given the high degree of structural homology between the two proteins. The increased selectivity for stromelysin-1 appears to be driven by (1) increased favorable van der Waals interactions, (2) increased favorable Coulombic interactions, and (3) decreased unfavorable total electrostatic energies (Coulombic plus desolvation).

Introduction

Matrix metalloproteinases (MMPs) are zinc dependent enzymes involved in a multitude of physiological processes including embryonic development, wound repair, and tissue remodeling.[1−4] Specific MMPs target the extracellular matrix (ECM) for degradation and promote the formation of new blood vessels (angiogenesis).[1] Given that angiogenesis is essential for the development and progression of tumor growth, MMP inhibitors could serve as effective anticancer agents.[1−3] However, despite the initial excitement offered by first generation MMP inhibitors to restrict invasive tumor growth and metastasis in a variety of animal models,[4,5] clinical trial results have been disappointing; no clinical efficacy in humans has been demonstrated.[2,5] Recent studies have shown that MMPs also appear to regulate the production of angiostatin, a potent angiogenesis inhibitor that inhibits tumor growth.[1,2,6,7] These findings suggest that more selective MMP inhibitors are crucial for the development of clinically effective chemotherapeutics.[1,8,9]

Several classes of compounds have been reported which bind to the active site residues in MMPs and effectively prevent normal substrate degradation. Compounds include peptidomimetic, nonpeptidomimetic, tetracycline, and bisphosphonate inhibitors.[4,10] Peptidomimeti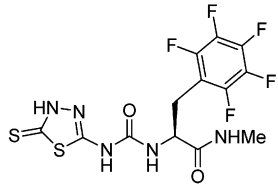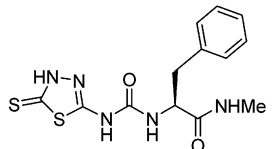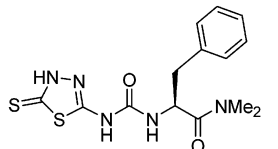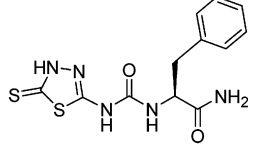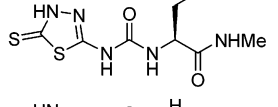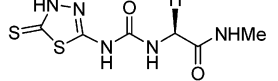cs were originally designed based on the amino acid sequence flanking the cleavage site in the natural substrate, collagen, for the MMP collagenase. Several nonpeptidomimetics have been guided through structure-based design[11] approaches using crystallographic information.[4,10] Structural studies have revealed that most inhibitors interact with MMP active site residues through an elaborate hydrogen-bond network and chelation of the active-site zinc.[4] Several zinc binding groups (ZBG) have been discovered which include a carboxylate, aminocarboxylate, sulfhydryl, hydroxamate, phosphonate, or phosphinate moiety.[4,10] Recently, 5-substituted-1,3,4-thiadozole-2-thione compounds have been reported that contain a novel ZBG where coordination occurs through the exocyclic sulfur of a thiadiazole group.[12] Structure−activity-relationship (SAR) studies have shown that thiadiazoles are selective for stromelysin-1 (MMP-3) over gelatinase-A (MMP-2) with little or no affinity for collagenase (MMP-1).[12]

The dual roles that matrix metalloproteinases appear to play in cancer growth and metastasis[1,5] highlight the need for studies that address a physical basis for selective inhibition of specific MMPs. In this report we have used computational modeling techniques to develop, refine, and validate simulation protocols and methods that can be used in the design of anticancer agents targeting the MMPs. We have focused on two specific MMPs, stromelysin-1 and gelatinase-A, since both have been implicated in breast cancer,[13,14] crystallographic structures of protein−ligand complexes are available,[15,16] and structure−activity data have been reported.[12] Although many MMPs are overexpressed in

---

* Corresponding author. E-mail: kuntz@cgl.ucsf.edu.
† Current address: Accelrys Inc., 9685 Scranton Road, San Diego, CA 92121-3752.

Table 1. Inhibition of Stromelysin-1 (str) and Gelatinase-A (gel) by Thiadiazole Ureas[a]

No.	Structure	str K_i	gel K_i	str ΔG_{bind} exptl	gel ΔG_{bind} exptl
70	PNU-142372	0.018	3.0	−10.57	−7.53
46	PNU-107859	0.71	3	−8.39	−6.15
57		2.3	226	−7.69	−4.97
56		3.3	>200	−7.48	>−5.05
29a		31	>200	−6.15	>−5.05
45		166	>100	−5.16	>−5.46

[a] K_i values in μM from ref 12. Estimated experimental binding energies $\Delta G_{exptl} \approx RT \ln(K_i)$ in kcal/mol at 25 °C.

breast cancer tissue and tumor cell lines,[13,14] stromelysin-1, in particular, has been shown to promote mammary carcinogenesis in mice[17,18]

Computer simulations of 5-substituted-1,3,4- thiadiazole-2-thiones (Table 1) with both stromelysin-1 and gelatinase-A have been performed in order to estimate free energies of binding for comparison with experiment. Aims of this research include (1) the development of generalized protocols and methods for continuum-based computer simulations (no explicit water) for systems with metallo centers, (2) the accurate prediction of binding affinities and selectivities of thiadiazole inhibitors with MMPs in comparison with experimental data, and (3) the elucidation of the basis for selectivity between MMPs through interpretation of the structural and energetic results from the simulations. By accurately modeling known MMP−ligand systems, new, selective, and potent MMP inhibitors can be proposed with greater confidence.

To estimate binding affinities and selectivities, we are using the MM-GBSA and MM-PBSA analysis techniques recently proposed by Srinivasen et al.[19] and reviewed by Kollman and co-workers.[20,21] To date, the MM-PBSA method has been applied to several protein−ligand systems in order to estimate free energies of binding for comparison with experiment; avidin (N = 9),[22] HIV reverse transcriptase (N = 12),[23] neuraminidase (N = 4),[24] cathepsin D (N = 7),[25] Sem-5 (N = 8),[26] growth factor receptor binding protein 2 (N = 5),[27] and stromelysin-1 with carboxylate ligands (N = 6).[28]

Although good correlation to experiment was obtained in many of the prior MM-PBSA studies, larger and more diverse data sets should be considered in order to further validate and test the utility of the method; in this report we are studying a different class of ligands (thiadiazoles) with stromelysin-1. In addition, prior MM-PBSA and MM-GBSA analysis have used molecular dynamics (MD) simulations with explicit water in order to generate the ensemble of coordinates (snapshots) used in subsequent binding affinity calculations;[22−28] the present study will evaluate the utility of using trajectories generated with a generalized Born continuum model (GB-MD). The motivation for using GB-MD is 2-fold: (1) in general, increased sampling for the ligand and protein would be expected from continuum simulations in comparison to explicit water simulations of the same length, and (2) in practice, shorter continuum simulations might be employed to compute thermodynamic and structural quantities that could only be obtained from much longer explicit solvent MD runs.

Theoretical Methods

Structure-based drug design using computational methods continues to hold great promise as simulation

methods and protocols become more refined and computers become more powerful. Of particular interest are simulation methods that accurately estimate free energies of binding (ΔG_{bind}) between small druglike molecules and a target protein without resorting to more rigorous and very CPU intensive methods of free energy perturbation (FEP) and thermodynamic integration (TI) techniques.[29] The recently reported MM-PBSA method[19−21] is faster by at least a factor of 10 than more traditional FEP or TI techniques and does not require any experimental data or fitting of parameters as in the Åqvist linear response (LR)[30] and extended linear response (ELR)[31−34] simulation methods. MM-PBSA is easily applicable to a wide range of diverse ligands.

In the original MM-PBSA formalism,[20,21] the total free energy of the system (G) is computed according to eq 1.

$$G = G_{polar} + G_{nonpolar} + E_{mm} - TS \qquad (1)$$

Here, a polar solvation energy term G_{polar} is computed in continuum solvent using a finite Poisson−Boltzmann (PB) model and a nonpolar solvation energy term $G_{nonpolar}$ is computed from a solvent-accessible surface area (SASA) calculation using eq 2 for each isolated state (receptor, ligand, or complex).[20,21]

$$G_{nonpolar} = (0.00542*SASA) + 0.92 \qquad (2)$$

Alternatively, a Generalized Born (GB) model may be used to estimate G_{polar}, yielding a method called MM-GBSA.[21] The E_{mm} term in eq 1 is a sum of the electrostatic (Coulombic), van der Waals (Lennard−Jones), and internal energies (bonds, angles, and dihedrals). Entropic effects may be included (TS term) where T is the temperature and the entropy S is typically estimated based on classical statistical formulas and normal-mode analysis of representative snapshots of energy-minimized structures from a molecular dynamics (MD) trajectory. The binding free energy is then estimated from eq 3.[20,21]

$$\Delta G_{bind} = G_{complex} - (G_{protein} + G_{ligand}) \qquad (3)$$

Hereafter, a distinction is made between MM-GBSA/PBSA results containing the $T\Delta S$ term ($\Delta G_{MM-GBSA+E}$) versus results without solute entropy estimates ($\Delta G_{MM-GBSA}$).

A MD simulation with explicit solvent is typically performed for each ligand bound to the protein to yield snapshots containing representative structures of the system(s),[20−28] although in the present research no explicit water was used in the simulation. Free energies (G), for each species, complex, protein, and ligand, are estimated with eq 1 using a set of Cartesian coordinates from a given trajectory snapshot and the difference (eq 3) gives ΔG_{bind}. Multiple snapshots are taken during the course of the MD trajectory to yield an average ΔG_{bind}. For $G_{complex}$, bulk explicit solvent (if present) is removed, while for $G_{protein}$ and G_{ligand} explicit solvent and the ligand or the protein are removed, respectively.[20,21] Specific individual water molecules suggested to be important for ligand recognition may be retained in the coordinate files used in the posttrajectory analysis.[24]

It is important to note that the sum of G_{polar} (PB or GB energies) and $G_{nonpolar}$ (SASA based) terms in the

MM-PB/GBSA expression (eqs 1 and 3) is considered to be a reasonable estimate of the free energy of hydration (ΔG_{hyd}) for a given molecule if, as is commonly assumed, dielectric constants of 1 (gas-phase) and 80 (water-phase) are specified as shown in eq 4.[35−37]

$$\Delta G_{hyd} = G_{polar} + G_{nonpolar} \qquad (4)$$

One way to evaluate the accuracy of theoretical methods and partial charge models for use in macromolecular simulations is to compare experimental ΔG_{hyd} values with calculated results. Results from ΔG_{hyd} calculations, obtained from PBSA and GBSA methods using the recently reported AM1-BCC[38,39] partial charge model, are presented below.

Computational Details

System Setups. Crystallographic structures of stromelysin-1 (pdb entry 1USN)[15] complexed with a thiadiazole inhibitor PNU-107859 (Table 1, compound **46**) and gelatinase-A (pdb entry 1QIB)[16] complexed with a hydroxamate inhibitor were used as starting coordinates for the present simulations. No crystallographic structure of gelatinase-A complexed with a thiadiazole inhibitor is currently available. Five analogues of compound **46** were manually constructed using the crystallographic coordinates of the stromelysin-1 complex (1USN) as a guide with the MOE program.[40] Analogues **70**, **57**, **56**, **29a**, and **45** from Jacobsen et al.[12] were chosen to (1) provide a reasonable range of experimental free energies of binding (Table 1) for comparison with experiment, and (2) be structurally similar to or smaller than the parent compound **46**. Using structurally similar compounds facilitates the construction of each protein−ligand complex and helps ensure that the ligands are placed in a reasonable starting conformation.

To generate models of the thiadiazoles bound to gelatinase-A, the enzyme was first superimposed to the stromelysin-1 coordinate frame through a rigid body translation and rotation which minimized the root-mean-square deviation (rmsd) between C_α carbons for residues 164−170, 194−206 (rmsd = 0.17Å). Visual inspection of the superposition results, for residues that line the binding pocket, guided the final choice as to which C_α carbons were used in the coordinate transformation. Thiadiazole−gelatinase-A complexes were then generated by simply deleting the stromelysin-1 receptor atoms while retaining the ligand coordinates for each of the six analogues. The final alignment (Figure 1, right) highlights the gross structural similarity between the stromelysin-1 (green tube) and gelatinase-A (blue tube) enzymes, especially in the vicinity of bound ligand PNU-107859 (red) and the coordinated zinc ion (magenta); a molecular surface representation of stromelysin-1 is also shown (Figure 1, left). An alternative approach would have been to use a complex of stromelysin-1 without PNU-107859 and build in the six thiadiazoles as done for the gelatinase-A setups. Although the original gelatinase-A coordinates were obtained from a cocrystal complex that did not contain a thiadiazole inhibitor, the energy minimizations and molecular dynamics equilibration procedures should remove any initial memory that might bias the stromelysin-1 calculations.

For the simulations, two zinc and three calcium ions common to both crystallographic complexes were retained but crystallographic waters were removed. His residues were singly protonated at either the epsilon (Nϵ) or delta nitrogen position (Nδ) to maximize coordination with zinc. One residue distal from each binding site was made neutral to enforce an overall charge of zero for the systems (Glu126 in stromelysin-1, Asp126 in gelatinase-A), otherwise AMBER7 default protonation states were employed.[41]

Standard PARM99[42] force field parameters were assigned to the protein, augmented by the Stote et al. nonbonded zinc model ($q = +2$ e$^-$, $\sigma = 1.7$ Å, $\epsilon = 0.67$ kcal/mol),[43] using the
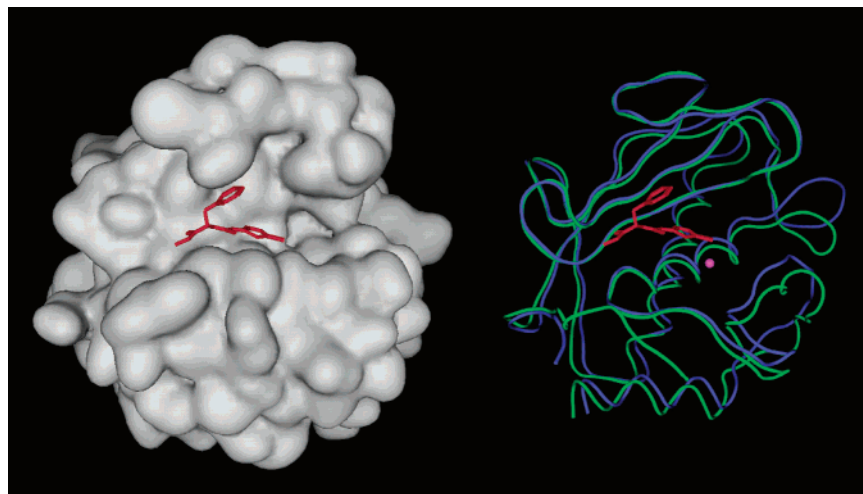
Figure 1. Left: Molecular surface of stromelysin-1 in gray showing ligand **46** in red. Right: Overlay of stromelysin-1 (green tube, pdb entry 1USN) and gelatinase-A (blue tube, pdb entry 1QIB) showing ligand **46** (red) and coordinated catalytic zinc ion (magenta). The two proteins were aligned using C_α carbons from residues 164−170 and 194−206 (0.17 Å rmsd difference).

LEAP program in AMBER7.[41] The Stote model was shown to yield the best overall results out of eight zinc parameter sets tested for docking ligands to thermolysin[44] and, more recently, MM-PBSA calculations have used the nonbonded model to rank binding energies for six known carboxylate ligands of stromelysin-1 in reasonable agreement with experiment.[28] For the ligands, GAFF[41] force fields parameters and AM1-BCC[38,39] partial charges were assigned using the ANTECHAMBER program as implemented in AMBER7.[41] Using this procedure, twelve simulation-ready systems were constructed each containing one of six ligands, that only differed in initial receptor (stromelysin-1 or gelatinase-A) coordinates.

Generalized Born Molecular Dynamics Simulations (GB-MD). A two-stage conjugant gradient energy minimization protocol was applied to each protein−ligand complex prior to the MD simulations. First, a minimization was performed for each system in which only the receptor heavy atoms were restrained to their crystallographic positions using a harmonic potential (force constant = 1000.0 kcal/mol Å²). A second restrained minimization was then performed using a much weaker force constant = 5.0 kcal/mol Å² in which only the protein main-chain atoms (C_α, C, N) were restrained. Both minimizations employed a distance dependent dielectric constant (4r) and loose tolerance for convergence (drms = 0.1 kcal/mol Å).

After the minimizations, molecular dynamics simulations were initiated without explicit water using the pairwise GB continuum solvent model of Hawkins and co-workers[45,46] implemented in the SANDER module of AMBER7. Simulations employed a 1 fs time step for 40010 steps corresponding to a total of 40.01 ps of GB-MD. The final desired temperature of 298 K was obtained by requesting a heating cycle from 0 to 298 K over the course of the first 5000 MD steps with temperature regulation maintained via coupling to an external heat bath using the Berendsen scheme[47] and a coupling time constant tautp = 1.0 ps. Protein main chain atoms were lightly restrained using a weak harmonic force constant = 5.0 kcal/mol Å², and the SHAKE[48] algorithm was applied to constrain bonds involving hydrogen atoms. Dielectric constants of 1 (interior) and 80 (exterior) were employed in all GB-MD simulations.

Average structural and energetic quantities used to estimate binding affinities for the MMP inhibitors and selectivities between stromelysin-1 and gelatinase-A were computed using 201 snapshots from the last 20.01 picoseconds of the MD trajectory as described below. Due to the computational expense, solute entropies were computed using six energy-minimized snapshots. No cutoff (cutoff = 999 Å) was employed during the GB-MD simulations.

MM-GBSA Processing. Following the extraction of coordinates representing individual species (complex, receptor, or ligand), from the GB-MD trajectory of each protein−ligand complex, the various MM-PB/GBSA energy terms in eq 1 were computed as follows. Electrostatic (E_{coul}), van der Waals (E_{vdw}), and internal energies were obtained using the SANDER module in AMBER7. Polar energies (G_{polar}) were obtained from the DelPhi[37] (PB energies), and AMBER7[41] (GB energies) programs using dielectric constants of 1 and 80 to represent gas and water phases, respectively. For the PB and GB calculations, the same coordinates, charges, and radii (mbondi)[49] were used. Nonpolar energies ($G_{nonpolar}$) were determined from eq 2 using SASAs computed with the MOLSURF[41] program. Solute entropies S were estimated using the NMODE module in AMBER6. Prior to the normal mode calculations, each species (complex, receptor, or ligand) was subjected to a conjugant gradient energy minimization using a distance dependent dielectric (4r) and tight convergence tolerance drms = 1.0×10^{-5} kcal/mol Å.

Results and Discussion

Free Energies of Hydration. The suitability of using AM1-BCC charges for the MMP ligands was tested through computation of free energies of hydration (ΔG_{hyd}) for model systems consisting of 410 neutral organic molecules using eq 4. The present data set was taken from Bordner et al.[50] which includes a three-dimensional structure for each compound along with the associated experimental log gas/water value as originally compiled by Abraham and co-workers.[51] Figure 2 compares experimental and theoretical free energies of hydration, computed using eq 4, obtained using AM1-BCC partial charges from PBSA ($r^2 = 0.80$) and GBSA ($r^2 = 0.77$) calculations. Two points may be noted about the ΔG_{hyd} results in Figure 2: (1) the excellent correlation with experimental free energies of hydration lends support for the use of AM1-BCC partial charges for the ligands, and (2) the nearly identical results obtained from the much faster GB calculations provide support for using GB derived G_{polar} energies for protein−ligand binding studies.

Continuum Trajectory Stability. To gauge whether the GB-MD simulations were stable and converged, energetic and structural properties were monitored during the course of the trajectories as illustrated in Figure 3 for compound **46** with stromelysin-1. In Figure 3, despite the short simulation times, instantaneous properties appear to be well converged before the data
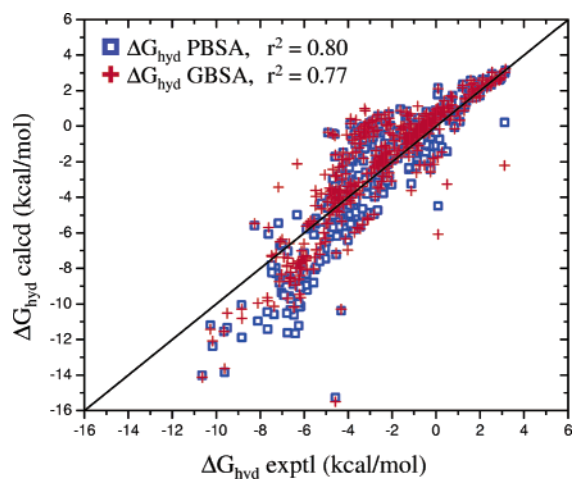
Figure 2. Predicted free energies of hydration (ΔG_{hyd} calcd) computed using eq 4 from PBSA (□) and GBSA (+) calculations vs experiment (ΔG_{hyd} exptl) for 410 neutral organic molecules[50] using AM1-BCC charges.

collection phase starting at 20.01 ps. Standard errors of the mean (sem) for ligand **46** with stromelysin-1 computed from the last 201 snapshots are low: $\Delta G_{MM-GBSA}$ = 0.13 kcal/mol, temp = 0.25 K (Figure 3a), ΔE_{vdw} = 0.13 kcal/mol, ΔE_{coul} = 0.25 kcal/mol, ΔG_{polar} = 0.21 kcal/mol, and $\Delta G_{nonpolar}$ = 0.005 kcal/mol (Figure 3b). Simulation results for the ligands with gelatinase-A are also well converged; standard errors of the mean for all properties, with the exception of the $T\Delta S$ terms, are very low (Table 2).

Structural properties were also monitored by computing the root-mean-square deviation (rmsd) between snapshots obtained during the course of the GB-MD trajectory and the original starting coordinates as illustrated in Figure 3c. Here, for ligand **46** with stromelysin-1, instantaneous rmsds (excluding hydrogen atoms) were computed for all heavy atoms (Figure 3c, top), protein backbone main chain atoms C_α, C, N (Figure 3c, middle), and ligand heavy atoms (Figure 3c, bottom). As noted above, a weak harmonic potential was applied during the current GB-MD simulations to bias the backbone main-chain atoms toward the crystallographic coordinates. The focus is on obtaining short, well-behaved, and converged simulations that achieve a reasonable amount of sampling for the ligands and amino acid side-chains about the initial crystallographic coordinates. Despite the harmonic restraint, simulation using the above protocols show a reasonable amount of backbone motion (Figure 3c middle), with rmsd fluctuations on the order of those observed during explicit water MD simulations for other systems.[52]

Zinc Coordination. The challenges associated with modeling protein systems containing zinc are well-known.[43] For this reason, the coordination states for both zinc ions were monitored during the course of the GB-MD simulations. Recently, MM-PBSA results have been reported from explicit water MD simulations for carboxylate MMP ligands with stromelysin-1 which invariably resulted in an octahedral coordination for the catalytic zinc ion in contrast to the tetrahedral coordination state observed in the crystal structure.[28]

In the present work, the correct tetrahedral geometry was maintained for the structural zinc (Zn2) with coordination neighbors His151@NE2, His166@NE2,
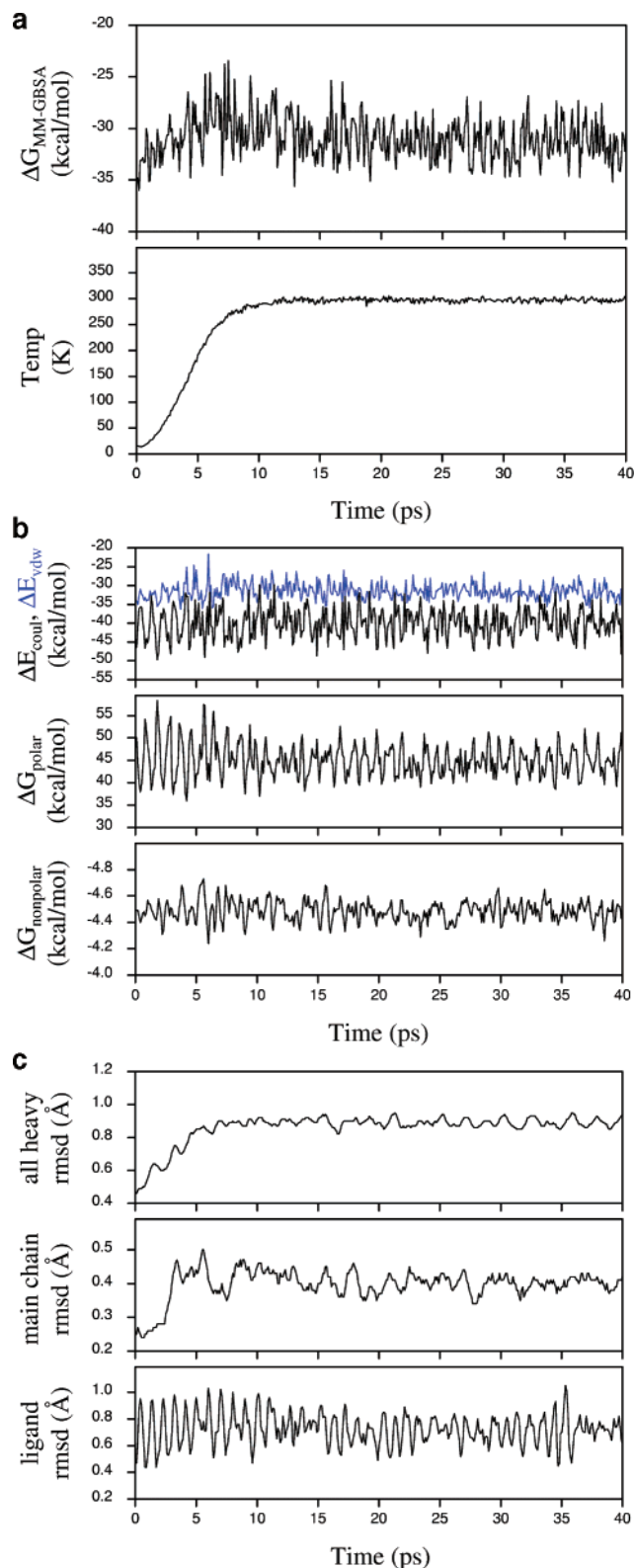
Figure 3. Instantaneous results from GB-MD simulations of ligand **46** with stromelysin-1 plotted vs time. (a) Temperature in Kelvin and $\Delta G_{MM-GBSA}$ sum (ΔE_{vdw} + ΔE_{coul} + ΔG_{polar} + $\Delta G_{nonpolar}$) in kcal/mol, (b) individual components ΔE_{vdw}, ΔE_{coul}, ΔG_{polar}, $\Delta G_{nonpolar}$ in kcal/mol, (c) root-mean-square deviation (rmsd) in angstroms (Å) between snapshots from the GB-MD simulations and initial starting coordinates for all heavy atoms (top), protein backbone main chain atoms C_α, C, N (middle), and ligand heavy atoms (bottom).

His179@ND1, and Asp153@CG during the course of the simulations, as illustrated in Figure 4a which is repre-

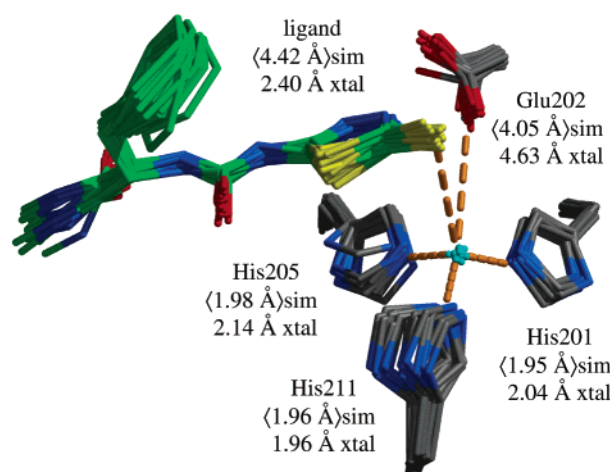**Table 2.** Contributions toward Calculated Free Energies of Binding (ΔG_{bind} calcd) from GB-MD Simulations and MM-GBSA Processing for Thiadiazoles with Stromelysin-1 (str) and Gelatinase-A (gel)[a]

system	ΔE_{vdw} (N = 201) A	ΔE_{coul} (N = 201) B	ΔG_{polar} (N = 201) C	$\Delta G_{nonpolar}$ (N = 201) D	$T\Delta S$ (N = 6) E	$\Delta E_{electro} =$ B+C+D	$\Delta G_{MM-GBSA} =$ A+B+C+D	$\Delta G_{MM-GBSA+E} =$ A+B+C+D+E	ΔG_{bind} exptl ≈ $RT \ln(K_i)$[b]
str **70**	-32.84 ± 0.15	-39.48 ± 0.27	41.48 ± 0.21	-4.56 ± 0.01	-14.87 ± 2.54	-2.56	-35.40 ± 0.14	-20.54 ± 2.54	-10.57
str **46**	-31.78 ± 0.13	-39.74 ± 0.25	44.63 ± 0.21	-4.48 ± 0.01	-18.52 ± 3.09	0.41	-31.37 ± 0.13	-12.84 ± 3.09	-8.39
str **57**	-30.73 ± 0.14	-40.36 ± 0.25	43.33 ± 0.20	-4.45 ± 0.01	-20.96 ± 1.87	-1.48	-32.21 ± 0.12	-11.25 ± 1.87	-7.69
str **56**	-29.34 ± 0.14	-37.51 ± 0.25	43.34 ± 0.21	-4.25 ± 0.01	-16.89 ± 1.36	1.58	-27.76 ± 0.13	-10.87 ± 1.37	-7.48
str **29a**	-25.11 ± 0.14	-40.67 ± 0.26	42.43 ± 0.20	-3.94 ± 0.01	-18.28 ± 0.87	-2.18	-27.30 ± 0.12	-9.02 ± 0.88	-6.15
str **45**	-22.94 ± 0.11	-38.70 ± 0.26	39.24 ± 0.20	-3.65 ± 0.01	-20.31 ± 1.57	-3.11	-26.05 ± 0.12	-5.74 ± 1.58	-5.16
	$r^2 = 0.86$	$r^2 = 0.004$	$r^2 = 0.15$	$r^2 = 0.82$	$r^2 = 0.48$	$r^2 = 0.03$	$r^2 = 0.87$	$r^2 = 0.97$	
gel **70**	-28.31 ± 0.13	-35.83 ± 0.24	43.22 ± 0.20	-4.25 ± 0.01	-21.28 ± 3.50	3.14	-25.17 ± 0.15	-3.90 ± 3.50	-7.53
gel **46**	-26.79 ± 0.15	-35.51 ± 0.25	44.80 ± 0.18	-4.16 ± 0.01	-21.42 ± 2.08	5.13	-21.65 ± 0.15	-0.22 ± 2.09	-6.15
gel **57**	-27.13 ± 0.13	-33.18 ± 0.30	42.26 ± 0.25	-4.19 ± 0.01	-18.31 ± 2.70	4.89	-22.24 ± 0.16	-3.93 ± 2.70	-4.97
gel **56**	-26.55 ± 0.12	-35.60 ± 0.25	45.28 ± 0.21	-4.04 ± 0.01	-15.15 ± 3.16	5.64	-20.92 ± 0.15	-5.77 ± 3.16	-5.05
gel **29a**	-20.94 ± 0.12	-36.10 ± 0.30	42.46 ± 0.23	-3.61 ± 0.01	-18.33 ± 1.03	2.75	-18.19 ± 0.14	0.14 ± 1.04	-5.05
gel **45**	-21.21 ± 0.12	-33.85 ± 0.26	39.89 ± 0.20	-3.51 ± 0.01	-14.93 ± 2.72	2.53	-18.68 ± 0.14	-3.75 ± 2.72	-5.46
	$r^2 = 0.24$	$r^2 = 0.14$	$r^2 = 0.02$	$r^2 = 0.21$	$r^2 = 0.47$	$r^2 = 0.06$	$r^2 = 0.55$	$r^2 = 0.00$	
total	$r^2 = 0.70$	$r^2 = 0.32$	$r^2 = 0.02$	$r^2 = 0.61$	$r^2 = 0.01$	$r^2 = 0.22$	$r^2 = 0.74$	$r^2 = 0.71$	

[a] All energies ± standard error of the mean in kcal/mol. [b] K_i values from ref 12.
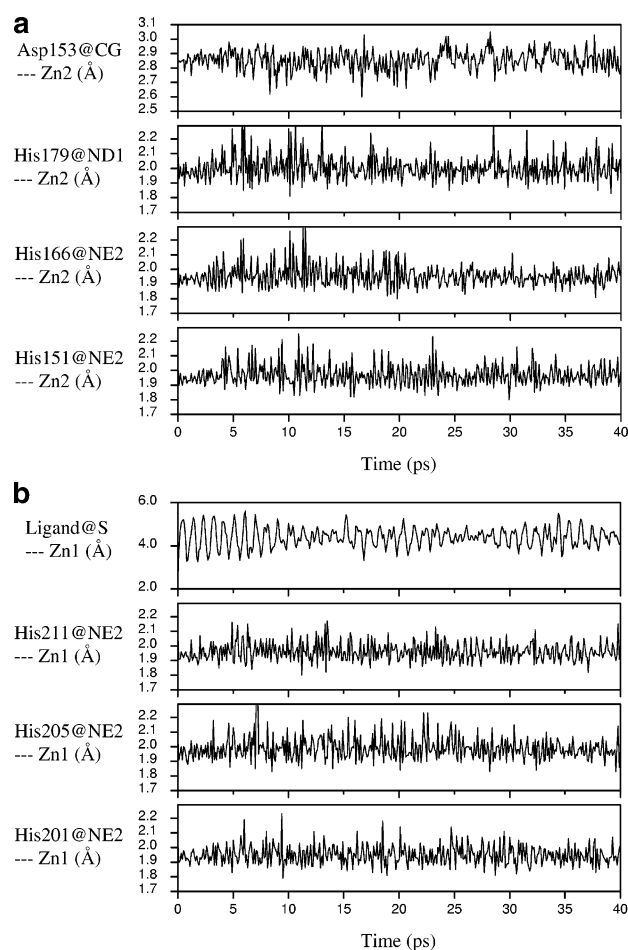
Figure 4. (a) Structural zinc (Zn2) and (b) catalytic zinc (Zn1) coordination distances for ligand **46** with stromelysin-1 from the last 20 ps of the GB-MD simulations.

Figure 5. Average and initial crystallographic zinc coordination distances for ligand **46** with stromelysin-1 (pdb entry 1USN) from the last 20 ps of the GB-MD simulations. Ligand **46** in green, protein residues in CPK colors, and catalytic zinc in cyan.

sentative; coordination distances oscillate about the observed crystal structure values. For the catalytic zinc (Zn1), however, deviation from the initial crystallographic distance is observed. In Figure 4b, instantaneous coordination distances for Zn1, with His201@NE2, His205@NE2, His211@NE1, and ligand exocyclic S, reveal that during the course of the simulation of ligand **46** with stromelysin-1, the average Zn1-ligand(S) distance is about 4.4 Å, much longer than the crystal structure value of 2.4 Å. Interestingly, the Zn1–ligand-

(S) distance exhibits a breathing not observed for the other coordinating residues (Figure 4b, top). Average zinc distances from the simulation of ligand **46** with stromelysin-1 are depicted in Figure 5 for comparison with experiment. A nearby Glu202 residue is also shown in Figure 5, whose average zinc–oxygen distance actually shortens by about 0.5 Å over the course of the simulation in comparison with the crystal. This glutamate, which also make bidentate hydrogen bonds with the thiadiazole NH, may partially compensate for any reduction in coordination energy lost by the elongation of the Zn1–ligand(S) distance.

To facilitate the discovery of second-generation MMP inhibitors, the suitability of using our restrained GB-MD procedure to model alternative ZBG should be tested. Ligands with carboxylate, aminocarboxylate, sulfhydryl, hydroxamate, phosphonate, or phosphinate[4,10] groups are expected to affect the metal ion and its coordination environment in different ways than the thiadiazole ZBG studied here and will therefore likely require different simulation protocols. Additional studies are needed to more fully resolve this issue.

Stromelysin-1 Binding. Free energies of binding were computed for stromelysin-1 (eqs 1 and 3) from
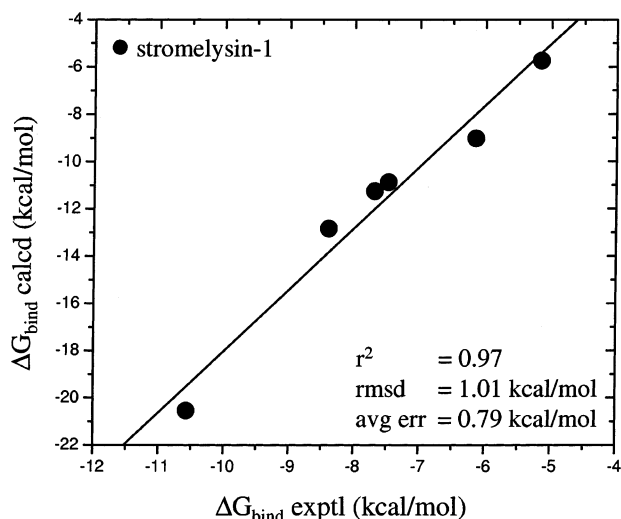
Figure 6. Predicted free energies of binding (ΔG_{bind} calcd) computed using eqs 1 and 3 from MM-GBSA calculations vs experiment (ΔG_{bind} exptl) for six ligands with stromelysin-1 (●).

Figure 7. Protein−ligand intermolecular Coulombic energies (ΔE_{coul}) vs opposing desolvation penalties ($\Delta G_{polar} + \Delta G_{nonpolar}$) for ligand **46** with stromelysin-1. Each point represents the energy obtained from 1 of 201 individual snapshots during the course of the GB-MD simulation.

snapshots saved every 0.10 ps from the final 20.01 ps of the GB-MD trajectories and presented in Table 2. For simulation results that include solute entropies ($\Delta G_{MM-GBSA+E}$), the best-fit line to the stromelysin-1 data yields a strong correlation coefficient with experiment ($r^2 = 0.97$), low standard deviation of 1.02 kcal/mol, and average unsigned error of only 0.79 kcal/mol (Figure 6). The excellent correlation with experiment is especially encouraging given the challenges presented: simulations are continuum-based, contain a metallo center, and are short (40.01 ps) by conventional standards.

Correlations of the individual energy terms with the experimental affinities were pursued to understand what drives binding (Table 2). The E_{vdw} energies ($r^2 = 0.86$) have the highest correlation with the variation in experimental affinities, followed by $G_{nonpolar}$ (0.82), $T\Delta S$ ($r^2 = 0.48$), G_{polar} ($r^2 = 0.15$), and finally E_{coul} ($r^2 = 0.004$). Given that separate simulations for unbound protein and ligand species were not performed, all intramolecular contributions (bonds, angles, dihedrals) to the total computed free energies cancel out. Therefore, E_{vdw} and E_{coul} terms are only composed of nonbonded interactions between the protein and ligand. For the stromelysin-1 simulations, including solute entropic contributions ($T\Delta S$) appears to be important as evident by a substantial increase in correlation with experiment, $r^2 = 0.87$ ($\Delta G_{MM-GBSA}$) to $r^2 = 0.97$ ($\Delta G_{MM-GBSA+E}$). In this study, PB methods were also used to estimate the ΔG_{polar} contribution to binding as discussed below. Given that both methods (GB vs PB) appear to yield free energies ($\Delta G_{MM-GBSA}$ vs $\Delta G_{MM-PBSA}$) in good agreement with experiment, the much faster GB calculations provide a valuable alternative.

During the course of the GB-MD simulations, the ΔE_{coul} and ΔG_{hyd} ($\Delta G_{polar} + \Delta G_{nonpolar}$) energies are highly anti-correlated ($r = -0.78$, $r^2 = 0.61$) as illustrated in Figure 7 for ligand **46**. As expected, favorable protein−ligand electrostatic energies (ΔE_{coul}) are approximately equal but opposite in sign to the desolvation penalties (ΔG_{hyd}) at each point in the GB-MD trajectory. The two competing effects nearly sum to zero,
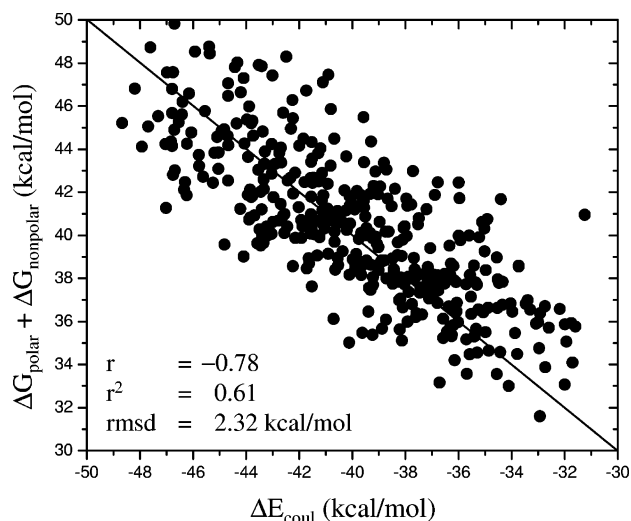
and the instantaneous free energies of binding are then dominated by the favorable ΔE_{vdw} and unfavorable $T\Delta S$ terms (Table 2). Remarkably, small differences in any average term can then account for the observed variation in binding, despite the fact that fluctuations in any given term may be large.

For comparison with the stromelysin-1 $\Delta G_{MM-GBSA+E}$ results, binding free energies were also computed using polar energies (G_{polar}) obtained from Poisson−Boltzmann (PB) calculations using the DelPhi[37] program. The PB calculations employed the same charges, radii, and coordinates as in the GB calculations. Not surprisingly, good agreement with experiment was observed ($r^2 = 0.90$ kcal/mol) using the G_{polar} results, from the PB calculations. The somewhat lower r^2 value with experiment compared to that obtained using the GB results ($r^2 = 0.97$ kcal/mol) may reflect the fact that the trajectories were originally generated using a GB-MD trajectory. Interestingly, as in the GB calculations, r^2 is diminished with the removal of the solute entropy term, $r^2 = 0.97$ ($\Delta G_{MM-GBSA+E}$) versus $r^2 = 0.77$ ($\Delta G_{MM-GBSA}$).

Selectivity: Stromelysin-1 versus Gelatinase-A. Experimentally the thiadiazoles are selective for stromelysin-1 over gelatinase-A (Table 1).[12] To understand the basis for this selectivity, free energies of binding were estimated for the six ligands with gelatinase-A adopting the same MM-GBSA and normal mode protocols as in the stromelysin-1 simulations (Figure 8, Table 2). Figure 8 shows the best fit line to the stromelysin-1 and gelatinase-A $\Delta G_{MM-GBSA+E}$ free energies which yield a strong correlation coefficient with experiment $r^2 = 0.71$, standard deviation = 3.32 kcal/mol, and average unsigned error = 2.45 kcal/mol. In each case, the simulation results correctly predict that a given ligand will bind more tightly to stromelysin-1 than gelatinase-A (Figure 8, Table 2), although, unlike the stromelysin-1 results, there is no linear correlation with the gelatinase-A experimental data alone. This might be a consequence of the fact that for ligands **56**, **29a**, and **45** with gelatinase-A (Table 1) there is uncertainty in the experimental measurements, and a comparison between
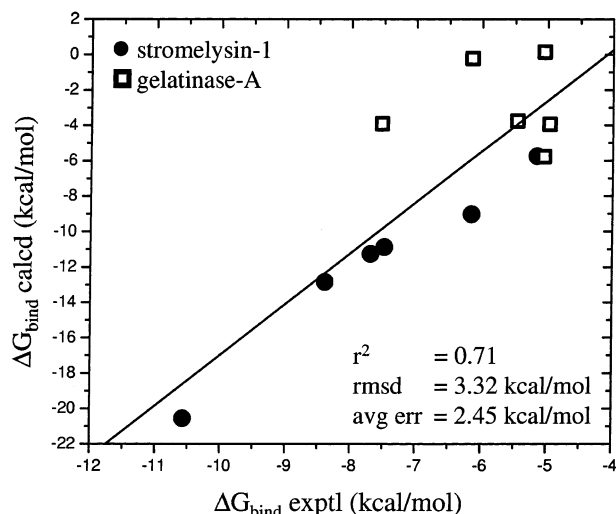
Figure 8. Predicted free energies of binding (ΔG_{bind} calcd) computed using eqs 1 and 3 from MM-GBSA calculations vs experiment (ΔG_{bind} exptl) for the six ligands with stromelysin-1 (●) and gelatinase-A (□).

best and worst binders (Table 2) shows a compressed experimental range for the ligands with gelatinase-A (−2.59 kcal/mol) compared to stromelysin-1 (−5.63 kcal/ mol). A small data range can make linear correlations of computer simulation results with experiment more difficult.[31] However, despite the experimental uncertainty, correlation with experiment for the ligands with gelatinase-A alone is restored ($\Delta G_{MM-GBSA}$ $r^2 = 0.55$) with the removal of the entropic term. In fact, the total correlation with experiment is improved for all the ligands with stromelysin-1 and gelatinase-A (r^2 from 0.71 to 0.74) without the entropic estimates. It should be emphasized that the $T\Delta S$ term is expected to be a crude approximation of only the solute entropy, and, if the simulations involve significant conformational sampling between conformational wells, the harmonic model is subject to failure.[19] Given that the fluctuations in $T\Delta S$ are much larger compared to the other energetic terms (Table 2), if resources and time allow, more snapshots should be used for the solute entropy estimates.

In total, the simulation results agree quite well with experiment and are useful in interpreting the experimental data. For example, ΔE_{vdw} and ΔE_{coul} energies (Table 2, columns A and B) for a given ligand are always less for gelatinase-A than for stromelysin-1, suggesting better charge complementarity and packing. The total electrostatic energies, embodied in the $\Delta E_{electro}$ term

($\Delta E_{electro} = \Delta E_{coul} + \Delta G_{polar} + \Delta G_{nonpolar}$), always oppose binding for gelatinase-A (2.53 to 5.13 kcal/mol, Table 2). In contrast, the stromelysin-1 ligands have favorable (−1.48 to −3.11) or much smaller unfavorable (0.41 to 1.58 kcal/mol) $\Delta E_{electro}$ energies (Table 2). Since the $\Delta G_{nonpolar}$ and ΔG_{polar} contributions are nearly constant for the ligands regardless of receptor, the ΔE_{coul} contribution dominates the $\Delta E_{electro}$ term. Given that solute entropic contributions ($T\Delta S$) for both data sets appear not to be a discriminating factor for selectivity among the enzymes, the dominant selectivity terms then become ΔE_{vdw} and ΔE_{coul}. Table 2 highlights the fact that for each ligand, increased favorable van der Waals and Coulombic interactions with stromelysin-1 are observed during the simulations in comparison to gelatinase-A.

Binding Site Differences. Figure 9 shows the alignment from stromelysin-1 (pdb entry 1USN) and gelatinase-A (pdb entry 1QIB) sequences obtained using the ClustalW program[53] and depicted using the BOXSHADE program.[54] The alignment highlights the overall sequence similarity, especially for residues that make contact with thiadiazole ligands (black circles). Binding site residues are defined as being within approximately 5 Å from any ligand atom. Of the 14 binding site residues highlighted in Figure 9, only four sequence changes are observed (underlined black circles). These four sequence changes, when coupled with structural information, can be used to interpret the experimental and computational results as illustrated in Figure 10. In Figure 10, three aromatic rings in stromelysin-1 make significant contact with the ligand compared with only one in the gelatinase-A structures. The large changes at position Phe86 (absent in gelatinase-A) and Phe210 (Glu in gelatinase-A) are expected to account for the reduction in favorable ΔE_{vdw} energies computed for the ligands with gelatinase-A (Table 2) compared to stromelysin-1 and probably contribute to the observed selectivity. Interestingly, in the gelatinase-A structure, the void created by the absence of residue 86 is partially filled by placement of a glutamate residue midway between the positions originally occupied by Phe aromatic rings in the stromelysin-1 structure through a change in the χ_1 angle of residue 210 from approximately 69° to 168° (Figure 10). For the remaining changes, the reduction in available contact surface for the ligands with Asn175 (stromelysin-1) versus Gly175 (gelatinase-A) would lead to reduced favorable van der Waals interactions of the compounds with gelatinase-
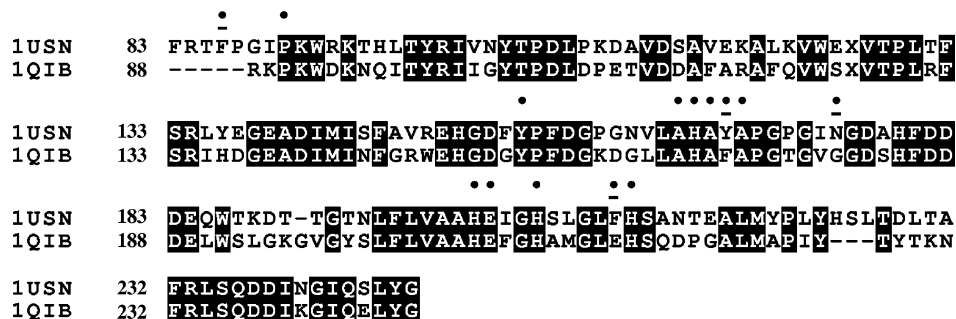
Figure 9. Stromelysin-1 (pdb entry 1USN) and gelatinase-A (pdb entry 1QIB) sequence alignment showing identical residues in black. The sequences were aligned using the ClustalW program,[53] and the picture was generated using the BOXSHADE program.[54] Residues within approximately 5 Å from the ligands are marked with a black circle (●). Sequence changes in binding site residues between the two MMPs are indicated with an underlined black circle (●).
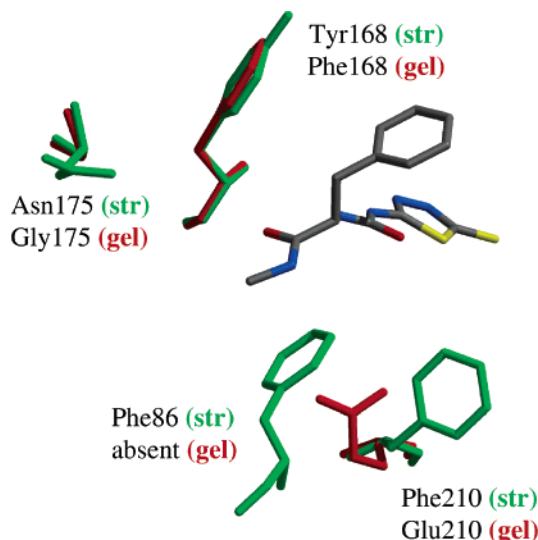
Figure 10. Binding site structural differences between stromelysin-1 (str, green) and gelatinase-A (gel, red). Ligand **46** in CPK colors; receptor and ligand coordinates are from pdb entries 1USN and 1QIB aligned using C_α carbons from residues 164–170 and 194–206 (0.17 Å rmsd difference).

A, while the minor Tyr to Phe swap at position 168 probably has little effect.

Conclusion

In this study we have used computational methods to estimate the free energy of binding for six ligands with stromelysin-1 and gelatinase-A using GB-MD simulations and MM-GBSA analysis. The predicted and experimental binding affinities ($\Delta G_{\text{MM–GBSA+E}}$) show strong correlation (Figure 8, $r^2 = 0.71$) which provides support for using continuum MD simulations, as an alternative to explicit water-based simulations, to generate the snapshots used in subsequent MM-PBSA/GBSA analysis. Convergence of the GB-MD simulations was carefully monitored through examination of instantaneous computed free energies of binding (Figure 3a), individual energy components (Figure 3b), rmsds from starting structures (Figure 3c), and zinc coordination states (Figures 4 and 5). Despite the short simulation times, all structural and energetic properties attributed to the GB-MD simulations appear to be well converged (Table 2). A limitation of the present method is that, unlike simulations containing explicit water, detailed solute–solvent interactions are absent. However, continuum methods are expected to have an added utility where increased sampling is desired and/or computational expense is of concern.

The variation in experimental binding affinities is best described using the $\Delta G_{\text{MM–GBSA}}$ results (Table 2). $\Delta G_{\text{MM–GBSA}}$ results contain terms representing the average intermolecular protein–ligand Coulombic and van der Waals energies (MM term), as well as a solvation term equivalent to the change in free energy of hydration for the system (GBSA term) upon complex formation. Interestingly, inclusion of solute entropic estimates ($\Delta G_{\text{MM–GBSA+E}}$) improved the correlation for the ligands with stromelysin-1 but diminished the correlation for the ligands with gelatinase-A. Removal of the solute entropies improved the total correlation,

consisting of all ligands complexed with both receptor, slightly ($\Delta G_{\text{MM–GBSA}}$, $r^2 = 0.74$ versus $\Delta G_{\text{MM–GBSA+E}}$, $r^2 = 0.71$).

In all cases, the simulation results correctly predict that a given ligand will bind selectively to stromelysin-1 rather than gelatinase-A (Figure 8, Table 2). Selectivity appears to be dominated by (1) increased favorable van der Waals interactions, (2) increased favorable Coulombic interactions, and (3) decreased unfavorable total electrostatic energies ($\Delta E_{\text{electro}} = \Delta E_{\text{coul}} + \Delta G_{\text{polar}} + \Delta G_{\text{nonpolar}}$) for the ligands with stromelysin-1. A comparison of the protein residues that line the different binding pockets (Figures 9 and 10) in the simulations reveals that three aromatic rings make significant contact with each ligand in stromelysin-1 versus one aromatic ring in gelatinase-A. These changes probably account for the reduction in favorable protein–ligand interactions.

The highly complex and various roles that specific MMPs appear to play in various stages of tumor growth and metastasis represent a major challenge for the development of clinically effective chemotherapeutics. In this report, we have participated toward this goal by demonstrating that MM-GBSA simulation methods can be used to effectively model MMP–ligand complexes and that the simulation results can be used to make free energy of binding predictions that correlate strongly with experimental affinities. In particular, the correct selectivity trends for ligands with stromelysin-1 versus gelatinase-A were obtained. The fact that clinical trial results for first generation MMP inhibitors have been disappointing highlights the need for additional computational studies that continue to address selectivity.

References

(1) Foda, H. D.; Zucker, S. Matrix metalloproteinases in cancer invasion, metastasis and angiogenesis. *Drug Discovery Today* **2001**, *6*, 478–482.
(2) Zucker, S.; Cao, J.; Chen, W. T. Critical appraisal of the use of matrix metalloproteinase inhibitors in cancer treatment. *Oncogene* **2000**, *19*, 6642–6650.
(3) Sternlicht, M. D.; Werb, Z. How matrix metalloproteinases regulate cell behavior. *Annu. Rev. Cell. Dev. Biol.* **2001**, *17*, 463–516.
(4) Whittaker, M.; Floyd, C. D.; Brown, P.; Gearing, A. J. H. Design and therapeutic application of matrix metalloproteinase inhibitors. *Chem. Rev.* **1999**, *99*, 2735–2776.
(5) Coussens, L. M.; Fingleton, B.; Matrisian, L. M. Matrix metalloproteinase inhibitors and cancer: trials and tribulations. *Science* **2002**, *295*, 2387–2392.
(6) Cornelius, L. A.; Nehring, L. C.; Harding, E.; Bolanowski, M.; Welgus, H. G.; Kobayashi, D. K.; Pierce, R. A.; Shapiro, S. D. Matrix metalloproteinases generate angiostatin: effects on neovascularization. *J. Immunol* **1998**, *161*, 6845–6852.
(7) O'Reilly, M. S.; Wiederschain, D.; Stetler-Stevenson, W. G.; Folkman, J.; Moses, M. A. Regulation of angiostatin production by matrix metalloproteinase-2 in a model of concomitant resistance. *J. Biol. Chem.* **1999**, *274*, 29568–29571.
(8) Purcell, W. T.; Rudek, M. A.; Hidalgo, M. Development of matrix metalloproteinase inhibitors in cancer therapy. *Hematol. Oncol. Clin. North Am.* **2002**, *16*, 1189–1227.
(9) Overall, C. M.; Lopez-Otin, C. Strategies for MMP inhibition in cancer: innovations for the post-trial era. *Nat. Rev. Cancer* **2002**, *2*, 657–672.
(10) Hidalgo, M.; Eckhardt, S. G. Development of matrix metalloproteinase inhibitors in cancer therapy. *J. Natl. Cancer Inst.* **2001**, *93*, 178–193.

(11) Kuntz, I. D. Structure-based strategies for drug design and discovery. *Science* **1992**, *257*, 1078−1082.

(12) Jacobsen, E. J.; Mitchell, M. A.; Hendges, S. K.; Belonga, K. L.; Skaletzky, L. L.; Stelzer, L. S.; Lindberg, T. J.; Fritzen, E. L.; Schostarez, H. J.; O'Sullivan, T. J.; Maggiora, L. L.; Stuchly, C. W.; Laborde, A. L.; Kubicek, M. F.; Poorman, R. A.; Beck, J. M.; Miller, H. R.; Petzold, G. L.; Scott, P. S.; Truesdell, S. E.; Wallace, T. L.; Wilks, J. W.; Fisher, C.; Goodman, L. V.; Kaytes, P. S.; et al. Synthesis of a series of stromelysin-selective thiadiazole urea matrix metalloproteinase inhibitors. *J. Med. Chem.* **1999**, *42*, 1525−1536.

(13) Garbett, E. A.; Reed, M. W.; Stephenson, T. J.; Brown, N. J. Proteolysis in human breast cancer. *Mol. Pathol.* **2000**, *53*, 99−106.

(14) Bartsch, J. E.; Staren, E. D.; Appert, H. E. Matrix metalloproteinase expression in breast cancer. *J. Surg. Res.* **2003**, *110*, 383−392.

(15) Finzel, B. C.; Baldwin, E. T.; Bryant, G. L., Jr.; Hess, G. F.; Wilks, J. W.; Trepod, C. M.; Mott, J. E.; Marshall, V. P.; Petzold, G. L.; Poorman, R. A.; O'Sullivan, T. J.; Schostarez, H. J.; Mitchell, M. A. Structural characterizations of nonpeptidic thiadiazole inhibitors of matrix metalloproteinases reveal the basis for stromelysin selectivity. *Protein Sci.* **1998**, *7*, 2118−2126.

(16) Dhanaraj, V.; Williams, M. G.; Ye, Q.-Z.; Molina, F.; Johnson, L. L.; Ortwine, D. F.; Pavlovsky, A.; Rubin, J. R.; Skeean, R. W.; White, A. D.; Humblet, C.; Hupe, D. J.; Blundell, T. L. X-ray Structure of Gelatinase a Catalytic Domain Complexed with a Hydroxamate Inhibitor. *Croat. Chem. Acta* **1999**, *72*, 575−591.

(17) Sternlicht, M. D.; Lochter, A.; Sympson, C. J.; Huey, B.; Rougier, J. P.; Gray, J. W.; Pinkel, D.; Bissell, M. J.; Werb, Z. The stromal proteinase MMP3/stromelysin-1 promotes mammary carcinogenesis. *Cell* **1999**, *98*, 137−146.

(18) Sternlicht, M. D.; Bissell, M. J.; Werb, Z. The matrix metalloproteinase stromelysin-1 acts as a natural mammary tumor promoter. *Oncogene* **2000**, *19*, 1102−1113.

(19) Srinivasan, J.; Cheatham, T. E.; Cieplak, P.; Kollman, P. A.; Case, D. A. Continuum solvent studies of the stability of DNA, RNA, and phosphoramidate − DNA helices. *J. Am. Chem. Soc.* **1998**, *120*, 9401−9409.

(20) Kollman, P. A.; Massova, I.; Reyes, C.; Kuhn, B.; Huo, S.; Chong, L.; Lee, M.; Lee, T.; Duan, Y.; Wang, W.; Donini, O.; Cieplak, P.; Srinivasan, J.; Case, D. A.; Cheatham, T. E. Calculating structures and free energies of complex molecules: combining molecular mechanics and continuum models. *Acc. Chem. Res.* **2000**, *33*, 889−897.

(21) Massova, I.; Kollman, P. A. Combined molecular mechanical and continuum solvent approach (MM-PBSA/GBSA) to predict ligand binding. *Perspect. Drug Discovery Des.* **2000**, *18*, 113−135.

(22) Kuhn, B.; Kollman, P. A. Binding of a diverse set of ligands to avidin and streptavidin: An accurate quantitative prediction of their relative affinities by a combination of molecular mechanics and continuum solvent models. *J. Med. Chem.* **2000**, *43*, 3786−3791.

(23) Wang, J.; Morin, P.; Wang, W.; Kollman, P. A. Use of MM-PBSA in reproducing the binding free energies to HIV-1 RT of TIBO derivatives and predicting the binding mode to HIV-1 RT of efavirenz by docking and MM-PBSA. *J. Am. Chem. Soc.* **2001**, *123*, 5221−5230.

(24) Masukawa, K. M.; Kollman, P. A.; Kuntz, I. D. Investigation of Neuraminidase-Substrate Recognition Using Molecular Dynamics and Free Energy Calculations. *J. Med. Chem.* **2003**, *46*, 5628−5637.

(25) Huo, S.; Wang, J.; Cieplak, P.; Kollman, P. A.; Kuntz, I. D. Molecular dynamics and free energy analyses of cathepsin D-inhibitor interactions: insight into structure-based ligand design. *J. Med. Chem.* **2002**, *45*, 1412−1419.

(26) Wang, W.; Lim, W. A.; Jakalian, A.; Wang, J.; Luo, R.; Bayly, C. I.; Kollman, P. A. An analysis of the interactions between the Sem-5 SH3 domain and its ligands using molecular dynamics, free energy calculations, and sequence analysis. *J. Am. Chem. Soc.* **2001**, *123*, 3986−3994.

(27) Suenaga, A.; Hatakeyama, M.; Ichikawa, M.; Yu, X.; Futatsugi, N.; Narumi, T.; Fukui, K.; Terada, T.; Taiji, M.; Shirouzu, M.; Yokoyama, S.; Konagaya, A. Molecular dynamics, free energy, and SPR analyses of the interactions between the SH2 domain of Grb2 and ErbB phosphotyrosyl peptides. *Biochemistry* **2003**, *42*, 5195−5200.

(28) Donini, O. A. T.; Kollman, P. A. Calculation and prediction of binding free energies for the matrix metalloproteinases. *J. Med. Chem.* **2000**, *43*, 4180−4188.

(29) Gohlke, H.; Klebe, G. Approaches to the description and prediction of the binding affinity of small-molecule ligands to macromolecular receptors. *Angew. Chem., Int. Ed. Engl.* **2002**, *41*, 2644−2676.

(30) Åqvist, J.; Medina, C.; Samuelsson, J.-E. A New Method For Predicting Binding Affinity in Computer-Aided Drug Design. *Protein Eng.* **1994**, *7*, 385−391.

(31) Rizzo, R. C.; Tirado-Rives, J.; Jorgensen, W. L. Estimation of Binding Affinities for HEPT and Nevirapine Analogues with HIV-1 Reverse Transcriptase via Monte Carlo Simulations. *J. Med. Chem.* **2001**, *44*, 145−154.

(32) Pierce, A. C.; Jorgensen, W. L. Estimation of Binding Affinities for Selective Thrombin Inhibitors via Monte Carlo Simulations. *J. Med. Chem.* **2001**, *44*, 1043−1050.

(33) Rizzo, R. C.; Udier-Blagovic, M.; Wang, D. P.; Watkins, E. K.; Kroeger Smith, M. B.; Smith, R. H., Jr.; Tirado-Rives, J.; Jorgensen, W. L. Prediction of activity for nonnucleoside inhibitors with HIV-1 reverse transcriptase based on Monte Carlo simulations. *J. Med. Chem.* **2002**, *45*, 2970−2987.

(34) Wesolowski, S. S.; Jorgensen, W. L. Estimation of binding affinities for celecoxib analogues with COX-2 via Monte Carlo-extended linear response. *Bioorg. Med. Chem. Lett.* **2002**, *12*, 267−270.

(35) Still, W. C.; Tempczyk, A.; Hawley, R. C.; Hendrickson, T. Semianalytical Treatment of Solvation For Molecular Mechanics and Dynamics. *J. Am. Chem. Soc.* **1990**, *112*, 6127−6129.

(36) Qiu, D.; Shenkin, P. S.; Hollinger, F. P.; Still, W. C. The GB/SA continuum model for solvation. A fast analytical method for the calculation of approximate Born radii. *J. Phys. Chem. A* **1997**, *101*, 3005−3014.

(37) Sitkoff, D.; Sharp, K. A.; Honig, B. Accurate Calculation of Hydration Free-Energies Using Macroscopic Solvent Models. *J. Phys. Chem.* **1994**, *98*, 1978−1988.

(38) Jakalian, A.; Bush, B. L.; Jack, D. B.; Bayly, C. I. Fast, efficient generation of high-quality atomic charges. AM1- BCC model: I. Methodol. *J. Comput. Chem.* **2000**, *21*, 132−146.

(39) Jakalian, A.; Jack, D. B.; Bayly, C. I. Fast, efficient generation of high-quality atomic charges. AM1-BCC model: II. Parametrization and validation. *J. Comput. Chem.* **2002**, *23*, 1623−1641.

(40) *MOE Version 2002.03*; Chemical Computing Group: Montreal, Canada.

(41) *AMBER Version 7*; University of California at San Francisco: San Francisco, CA.

(42) Wang, J. M.; Cieplak, P.; Kollman, P. A. How well does a restrained electrostatic potential (RESP) model perform in calculating conformational energies of organic and biological molecules? *J. Comput. Chem.* **2000**, *21*, 1049−1074.

(43) Stote, R. H.; Karplus, M. Zinc binding in proteins and solution: a simple but accurate nonbonded representation. *Proteins* **1995**, *23*, 12−31.

(44) Vaz, R. J.; Kuntz, I. D.; Meng, E. C. Evaluating nonbonded parameters for zinc in DOCK. *Med. Chem. Res.* **1999**, *9*, 479−489.

(45) Hawkins, G. D.; Cramer, C. J.; Truhlar, D. G. Pairwise Solute Descreening of Solute Charges from a Dielectric Medium. *Chem. Phys. Lett.* **1995**, *246*, 122−129.

(46) Hawkins, G. D.; Cramer, C. J.; Truhlar, D. G. Parametrized models of aqueous free energies of solvation based on pairwise descreening of solute atomic charges from a dielectric medium. *J. Phys. Chem.* **1996**, *100*, 19824−19839.

(47) Berendsen, H. J. C.; Postma, J. P. M.; Vangunsteren, W. F.; Dinola, A.; Haak, J. R. Molecular-Dynamics with Coupling to an External Bath. *J. Chem. Phys.* **1984**, *81*, 3684−3690.

(48) Ryckaert, J. P.; Ciccotti, G.; Berendsen, H. J. C. Numerical-Integration of Cartesian Equations of Motion of a System with Constraints − Molecular-Dynamics of N-Alkanes. *J. Comput. Phys.* **1977**, *23*, 327−341.

(49) Tsui, V.; Case, D. A. Molecular dynamics simulations of nucleic acids with a generalized born solvation model. *J. Am. Chem. Soc.* **2000**, *122*, 2489−2498.

(50) Bordner, A. J.; Cavasotto, C. N.; Abagyan, R. A. Accurate Transferable Model for Water, n-Octanol, and n-Hexadecane Solvation Free Energies. *J. Phys. Chem. B* **2002**, *106*, 11009−11015.

(51) Abraham, M. H.; Whiting, G. S.; Fuchs, R.; Chambers, E. J. Thermodynamics of Solute Transfer from Water to Hexadecane. *J. Chem. Soc., Perkin Trans. 2* **1990**, 291−300.

(52) Kuhn, B.; Kollman, P. A. A ligand that is predicted to bind better to avidin than biotin: Insights from computational fluorine scanning. *J. Am. Chem. Soc.* **2000**, *122*, 3909−3916.

(53) Thompson, J. D.; Higgins, D. G.; Gibson, T. J. Clustal W: Improving the Sensitivity of Progressive Multiple Sequence Alignment through Sequence Weighting, Position-Specific Gap Penalties and Weight Matrix Choice. *Nucleic Acids Res.* **1994**, *22*, 4673−4680.

(54) BOXSHADE Version 3.21; http://www.ch.embnet.org/software/ BOX_form.html.

JM030570K